

Nanoscale

Accepted Manuscript



This is an *Accepted Manuscript*, which has been through the Royal Society of Chemistry peer review process and has been accepted for publication.

Accepted Manuscripts are published online shortly after acceptance, before technical editing, formatting and proof reading. Using this free service, authors can make their results available to the community, in citable form, before we publish the edited article. We will replace this *Accepted Manuscript* with the edited and formatted *Advance Article* as soon as it is available.

You can find more information about *Accepted Manuscripts* in the [Information for Authors](#).

Please note that technical editing may introduce minor changes to the text and/or graphics, which may alter content. The journal's standard [Terms & Conditions](#) and the [Ethical guidelines](#) still apply. In no event shall the Royal Society of Chemistry be held responsible for any errors or omissions in this *Accepted Manuscript* or any consequences arising from the use of any information it contains.



3D Porous Ni-Cu Alloy Film for High-performance Hydrazine Electrooxidation

Ming Sun, Zhiyi Lu, Liang Luo*, Zheng Chang*, Xiaoming Sun

Received 00th January 20xx,
Accepted 00th January 20xx

DOI: 10.1039/x0xx00000x

www.rsc.org/

The structural design and catalyst screening are two most important factors for achieving exceptional electrocatalytic performance. Herein we demonstrate that constructing three-dimensional (3D) porous Ni-Cu alloy film is of great beneficial for improving hydrazine oxidation reaction (HzOR) performance. A facile electrodeposition process is employed to synthesize the Ni-Cu alloy film with a 3D hierarchical porous structure. As an integrated electrode for HzOR, the Ni-Cu alloy film exhibits superior catalytic activity and stability compared to the Ni or Cu counterparts. The synthesis parameters are also systematically tuned for optimizing the HzOR performance. The excellent HzOR performance of the Ni-Cu alloy film is attributed to the high intrinsic activity of Ni/Cu, the large electrochemical specific surface area, and the 3D porous architecture which offers a “superaerophobic” surface to effectively remove the gas product in a small size. It is believed that the Ni-Cu alloy film electrode possesses potential application in the direct hydrazine fuel cell as well as other catalytic fields.

Introduction

Direct hydrazine fuel cells (DHFCs) have been widely investigated as low-cost and clean power sources for future mobile and stationary applications due to their high energy and power densities, which both are much superior to conventional batteries.¹ DHFCs have many advantages including high theoretical potential (1.64 V), high theoretical energy density, easy storage, and in particular, the possibility of using non-noble metals as anode and cathode catalysts. While one of the key challenges for DHFCs is the development of low-cost catalysts for hydrazine oxidation reaction (HzOR) with superior catalytic activity as well as stability.

Electrode catalysts for hydrazine electrooxidation reaction have been studied as early as 1960's,²⁻⁴ and many efforts have been devoted to the development of new electrocatalysts.⁵⁻¹³ Cu is a potential low-cost and stable anode catalyst for DHFCs,¹⁴ for instance, Jia et al.⁸ created a nanoporous Cu film with a better catalytic performance than smooth Cu or Au films in HzOR. However, Cu is normally not as active as noble metals and other transition metals considering the intrinsic electroactivity of Cu.¹⁵ Our previous work¹⁶ revealed that the discontinuous three phase contact line afforded by creating the high surface porosity helped the nanostructured Cu array film to display much improved electrocatalytic performance in

HzOR, due to the significantly reduced adhesion force toward the gas products. The “superaerophobic” Cu array film demonstrated a better HzOR performance than the commercial 60% Pt/C catalyst and its power density in DHFC was as high as 160 mW cm⁻². In contrast to the tremendous progress in exploring various nanostructured catalysts, the management of the gas products on microscopic electrode surfaces received very limited attention. This process is actually of substantial importance because the gas slugs accumulated on the electrode surface may not only hinder the liquid fuels transport to the active sites, but also impose a high pressure in the flow field.¹⁷⁻²⁰ Therefore, the transition metals and alloys with “superaerophobic” surfaces will be developed for their highly efficient applications in HzOR and DHFCs.

Ni is a highly effective catalyst for HzOR but its stability is relatively weak, and thus pure Ni has been hardly applied due to the easy run-off of Ni.²¹ Nevertheless, the different alloys containing Ni displayed relatively better performances for persistent HzOR. In recent researches, Ni-based binary alloy catalysts such as Ni-Zn,^{22, 23} Ni-Co,^{24, 25} Ni-Pd,²⁶ Ni-Pt,²⁷ Ni-Zr²⁸ and Ni-Fe²⁹ were shown to efficiently promote hydrazine hydrate electrooxidation through alloying effect. For example, Sakamoto et al.³⁰ reported a high-performance Ni-La catalyst for HzOR at 60°C in 1 mol L⁻¹ hydrazine, with a current density of 48.9 to 759.5 A g⁻¹ according to the different percent of Ni. Yin et al.²⁸ synthesized a Ni-Zr alloy catalyst which exhibited a current density of 165 mA cm⁻² in 2 mol L⁻¹ hydrazine. Though these Ni alloy catalysts showed excellent performances in HzOR, they usually utilized high hydrazine concentration and reaction temperature. Moreover, the stability tests were lacking for most of them. Even with testing in a few reports,

^a State Key Laboratory of Chemical Resource Engineering, Beijing University of Chemical Technology, Beijing 100029, China. Tel.: +8610-64448751; E-mail: changzheng@mail.buct.edu.cn; luoliang@mail.buct.edu.cn. Electronic Supplementary Information (ESI) available: [SEM and XPS characterization results]. See DOI: 10.1039/x0xx00000x

the stabilities were relatively poor (generally less than 40%), as listed in Table S1.^{22, 23, 28-35} These motivated us to further study Ni-based alloy catalyst with high current density and long-term stability for applying in HzOR and DHFCs under moderate reaction conditions (including room temperature and dilute hydrazine).

In this work, the three-dimensional (3D) porous Ni-Cu alloy film fabricated by one-step electrodeposition process was used as the anode catalyst for HzOR in alkaline media, which showed an impressive catalytic performance at room temperature and a low hydrazine concentration of 0.1 mol L⁻¹. The HzOR involves four electrons to oxidize one hydrazine molecule and form nitrogen gas product in alkaline environment (see **Reaction 1**). The highly porous Ni-Cu alloy film showed a negligible adhesion force to the gas bubbles, resulting in small releasing size and fast removal of the as-formed nitrogen gas bubbles (**Fig. 1**). So the excellent HzOR performance of the Ni-Cu alloy film was attributed to the high intrinsic activity of Ni/Cu catalysts and 3D porous architecture with a "superaerophobic" surface.

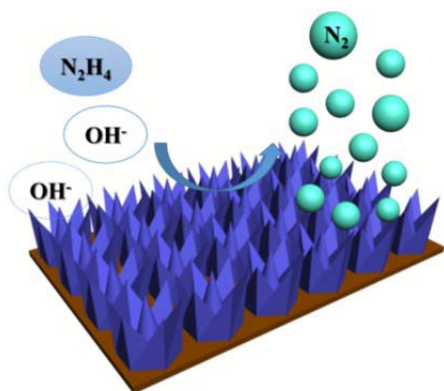


Fig. 1 Schematic illustration of the 3D porous Ni-Cu alloy film for HzOR.

Experimental

Preparation: The 3D porous Ni-Cu alloy films were fabricated by one-step electrodeposition process. First, the Cu foil substrates (1 cm × 1 cm) were pre-cleaned in 25% H₂SO₄ solution to remove surface oxides and then in ethanol for 5 min. After that, the electrodeposition process was performed on the dry pre-cleaned substrates in an aqueous electrolyte containing CuSO₄ · 5H₂O (0.10 mol L⁻¹), NiSO₄ · 6H₂O (0.54 mol L⁻¹), H₃BO₃ (0.30 mol L⁻¹) at a constant potential. The temperature was kept at 25 °C in a water bath during the whole electrodeposition process. The electrodeposition time varied at 100 – 600 s and the applied potential was tuned from -1.9 V to -1.2 V (vs. SCE) to investigate the optimized conditions. For

comparison, we fabricated a Ni array film by the same method except the electrolyte only containing NiSO₄ · 6H₂O (0.54 mol L⁻¹) and H₃BO₃ (0.30 mol L⁻¹), a nanostructured Cu array film (on Cu foil substrate) previously reported by us,¹⁶ a pure Cu foil and Ni foil as control samples.

Characterizations: The size and morphology of the samples were observed from scanning electron microscope (SEM, Zeiss Supra 55) operating at an accelerating voltage of 20 kV and transmission electron microscopy (TEM, FEI Technai G2F20 microscope) running at 200 kV. The samples for TEM were prepared by scraping Ni-Cu alloy powders from Cu foil substrates and ultrasonic vibration in ethanol, and then the suspensions were dropped onto carbon-enhanced copper grids and dried in air. X-ray photoelectron spectroscopy (XPS) measurements were performed using a Thermo Electro ESCALAB 250 instrument (Al Kα, 200 W). The experimental curves were fitted with a program that made use of a combination of Gaussian–Lorentzian lines. The X-ray diffraction (XRD) data were collected with a Shimadzu XRD-6000 diffractometer with Cu Kα radiation (λ=1.5418 Å). The nitrogen bubble releasing process was recorded by a high-speed CCD camera (AOS Technologies X-Motion) mounted on a microscope (OLYMPUS SZ-CTC). The interaction force between the gas bubbles and electrode interfaces was assessed by a high-sensitivity microelectromechanical balance system (Dataphysics DCAT11). All the experiments were repeated for more than five times.

Electrochemical Measurements: The HzOR performance was carried out at room temperature in a three-electrode glass cell connected to an electrochemical workstation (CHI 660D, Chenghua, Shanghai). Cyclic voltammetry and linear sweep voltammetry at a scan rate of 5 mV s⁻¹ were conducted in 3.0 mol L⁻¹ NaOH and 0.1 mol L⁻¹ N₂H₄ · H₂O solution using SCE as the reference electrode and Pt wire as the counter electrode. Alternating-current impedance measurements were carried out in the same configuration at -0.8 V from 10⁵ to 0.1 Hz and stability tests were operated at -0.6 V for 5000 s. Electrochemical surface area measurements were carried out in the same three-electrode system in 3.0 mol L⁻¹ pure NaOH solution.

Results and discussion

One-step electrodeposition process at a negative potential prior to hydrogen evolution reaction was employed to fabricate the 3D porous Ni-Cu alloy film. After electrodeposition at -1.8 V for 400 s, a black film was present on the Cu foil substrate. The top-view SEM image of the product (**Fig. 2a**) demonstrated that a rough surface with vertically aligned flower-like array film was uniformly formed on the Cu foil, and the high-magnification image (**Fig. 2b**) further revealed an average size of 400 nm of this flower-like nanostructure. The 3D array morphology created wide open spaces surrounded by adjacent nanostructures, resulting in the presence of high porosity. **Fig. 2c** shows the TEM image of an

individual nanostructure scraped off from the array film. Consistent to the SEM images, a multilayered flower-like nanostructure was observed, which was tightly deposited by small nanoparticles layer by layer towards the top. The corresponding XRD pattern (Fig. 2d) confirmed the crystal structure of pure Ni-Cu alloy. Except these sharp and strong peaks of Cu foil substrate, these diffraction peaks at about 45° , 52° and 76° were respectively indexed to the (111), (200) and (220) crystalline plane diffractions of Ni-Cu alloy considering they were exactly located at between the standard peaks of Cu (PDF#65-9026) and these of Ni (PDF#65-2865). Calculated from the XPS data in Fig. S1, the atomic proportions of Ni and Cu were respectively about 42.8% and 57.2%, i. e. Ni/Cu = 1/1.34, confirming the formation of Ni-Cu alloy structure. To further study surface state, the specific XPS spectra of Ni and Cu are shown in Fig. 2e and Fig. 2f. The Ni $2p_{3/2}$ spectrum could be split to three peaks, respectively attributed to Ni(0) (852.4 eV), Ni(II) (854.0 eV) and Ni(III) (855.8 eV)³⁶⁻³⁸, and the Cu $2p_{3/2}$ spectrum was split to two peaks corresponding to Cu(0) (932.2 eV) and Cu(I) (932.8 eV)^{39, 40}, which suggested that the Ni-Cu alloy were partly oxidized in the electrodeposition process though these oxides were silent in the XRD pattern. In summary, these results unambiguously proved that the 3D porous Ni-Cu alloy film was successfully fabricated by the one-step electrodeposition process.

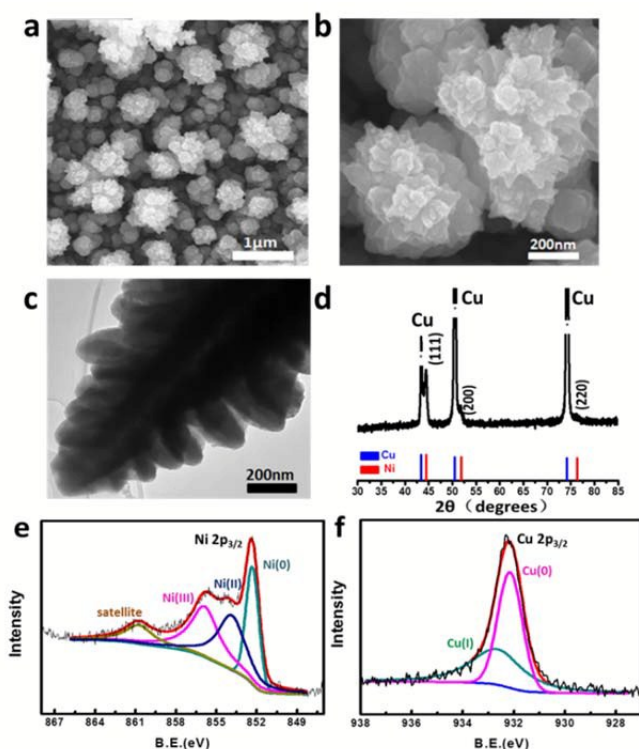


Fig. 2 a) top-view SEM image; b) high-magnification SEM image; c) TEM image; d) XRD pattern; e) Ni $2p_{3/2}$ and f) Cu $2p_{3/2}$ XPS data of the Ni-Cu alloy film.

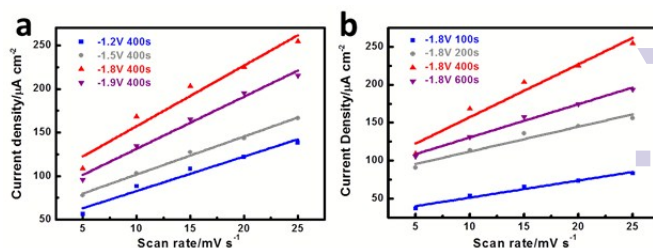


Fig. 3 Electrochemical surface area comparison of the Ni-Cu alloy films prepared under different conditions: a) different deposition potentials from -1.2, -1.5, -1.8 to -1.9 V for a deposition time of 400 s; b) different deposition times from 100, 200, 400 to 600 s at a deposition potential of -1.8 V.

As we know, the electrodeposition products are sensitive to experimental conditions, such as applied potential, time, temperature, concentration and so on. So a series of experiments were designed and processed to investigate these optimized conditions. Firstly, the electrodeposition process was performed at different applied potentials from -1.2 V, -1.5 V, -1.8 V to -1.9 V (vs. SCE) for the same deposition time of 400 s. We measured the current density evolution (vs. scan rate) of the Ni-Cu alloys, as shown in Fig. 3a. By calculating the slope of these lines, the electrochemical surface areas (ESAs) of the products prepared at -1.2, -1.5, -1.8 and -1.9 V were 3931, 4358, 6951 and 5982 $\mu\text{F cm}^{-2}$, respectively. The ESA increased as the potential increasing from -1.2 V to -1.8 V and then decreased as the potential increasing to -1.9 V. And the Ni-Cu alloy obtained at -1.8 V had also the largest deposition weight of 2.2 mg cm^{-2} compared to others. In their SEM images (Fig. S2a, S2b and S2c), the electrodeposition potential had an effect on the morphology of Ni-Cu alloys though all the products were porous flower-like films. With the potential increasing from -1.2 V to -1.8 V, the flower-like products gradually grew up, leading to the enhancement of porosity and deposition weight. When the potential increased to -1.9 V, moreover, however, the porosity and deposition weight of the Ni-Cu alloy film declined, probably related to peeling off of the alloys resulting from excessive metal deposition at higher potential. Subsequently, the electrodeposition process was performed at the applied potential of -1.8 V for the varied deposition time from 100 s to 600 s. The ESA results are shown in Fig. 3b, which revealed that the ESAs of the Ni-Cu alloys prepared for the deposition time of 100, 200, 400 and 600 s were 2249, 3264, 6951 and 4379 $\mu\text{F cm}^{-2}$, respectively. The ESAs sharply increased with the deposition time increasing from 100 s to 400 s owing to the enhancement of deposition amount of porous alloys with time extending, but then decreased once the time further increased to 600 s due to the negative effect of excessive deposited alloys. The SEM images of the products (Fig. S2d, S2e and S2f) suggested that the deposition time could influence the morphology and deposition weight of these porous flower-like Ni-Cu alloy. Thus 1.8 V and 400 s were chosen as the currently optimized electrodeposition conditions, and the optimal Ni-Cu alloy film with the 3D porous structure, large deposition weight and high

electrochemical surface area would be expected to perform a good HzOR performance.

We investigated the electrocatalytic performance of the 3D porous Ni-Cu alloy films for HzOR in 3.0 mol L⁻¹ NaOH solution with 0.1 mol L⁻¹ N₂H₄·H₂O. It should be noted that once the Ni-Cu alloy films with naturally oxidized surface were immersed in the hydrazine solution, several gas bubbles were generated on the working electrode surface suggesting that these surface metal oxides could be immediately reduced by hydrazine (leading to the presence of N₂ bubbles), and thus the electrocatalysts for HzOR were assured to be Ni(0)-Cu(0) alloys. For the catalytic performance comparison, the pristine Ni foil, Cu foil, nanostructured Cu array film synthesised according to our previous report¹⁶ (Fig. S3a) and Ni array film prepared under the similar conditions (Fig. S3b) were used as control samples. Their electrocatalyst performances for HzOR are shown in Fig. 4a, which indicated the Ni-Cu alloy film performed a significantly boosted current density enhancement for HzOR compared with other Cu or Ni samples. For instance, at the same potential of -0.6 V, the pristine Cu foil substrate only afforded a small current (≈17 mA cm⁻²), and the nanostructured Cu array film presented a 6 times higher current (≈110 mA cm⁻²) attributing to the porous structure with a “superaerophobic” surface.¹⁶ The Ni array film showed a 10 times higher current (≈175 mA cm⁻²) owing to the inherent activity of Ni though the pristine Ni foil hardly had activity. While the as-prepared Ni-Cu alloy film exhibited an 18 times higher current (≈300 mA cm⁻²). The high activity of the Ni-Cu alloy film was impressive, especially under moderate reaction conditions (room temperature and 0.1 mol L⁻¹ hydrazine). Moreover, the electrocatalytic performance of the Ni-Cu alloy film was closely dependent on the electrodeposition conditions, like deposition potential and time. As shown in Fig. 4b, by varying the electrodeposition potential from -1.2 V to -1.9 V, the HzOR performances of a series of Ni-Cu alloy films firstly increased until the potential reached -1.8 V and then declined as the potential further increasing to -1.9 V. In Fig. 4c, the HzOR performance of the Ni-Cu alloy film prepared at the deposition time of 400 s was better than any other sample with different deposition time varying from 100 s to 600 s. Thus the Ni-Cu alloy deposited at -1.8 V for 400 s presented the optimal HzOR property under the current conditions. This phenomenon was consistent with the previously discussed structure change, which demonstrated that the suitable porous structure, the enlarged electrochemical surface area and deposition weight could promote the electrochemical performance of the Ni-Cu alloy film. Finally, the stability tests of the Ni-Cu alloy film and control samples were carried out at a constant potential of -0.6 V and shown in Fig. 4d. The HzOR current density of the Ni-Cu alloy film was still as high as 250 mA cm⁻² after 5000 s, maintaining above 80% of the initial value. The stability was impressive and surpassed the most of previously reported Ni-based electrocatalysts for HzOR (as listed in Table S1). However, the stability of the Ni array film prepared in the similar conditions was relatively poor and the current density

sharply decreased to 50% in the first 30 s. As those previous reports,^{20, 41} the easy run-off of active Ni electrocatalysts restricted their applications in HzOR and DHFCs, but Cu alloying treatment could help to improve the stability of Ni-based electrocatalysts. Moreover, the Cu array film with a 3D porous structure also showed a good stability for HzOR with current density retention of 78% after 5000 s. It revealed that the Ni-Cu alloying treatment significantly improved not only the electrochemical activity but also the stability of Ni-based electrodes for HzOR, which might be related to the fixation of active Ni by Cu atoms in the Ni-Cu alloy structure. As shown in Fig. S4, even after the stability test for 5000 s, the Ni-Cu alloy film still presented a relatively steady structure and morphology like before. Therefore, the excellent electrochemical performance of the 3D porous Ni-Cu alloy film suggested a potential to apply in DHFCs in the future.

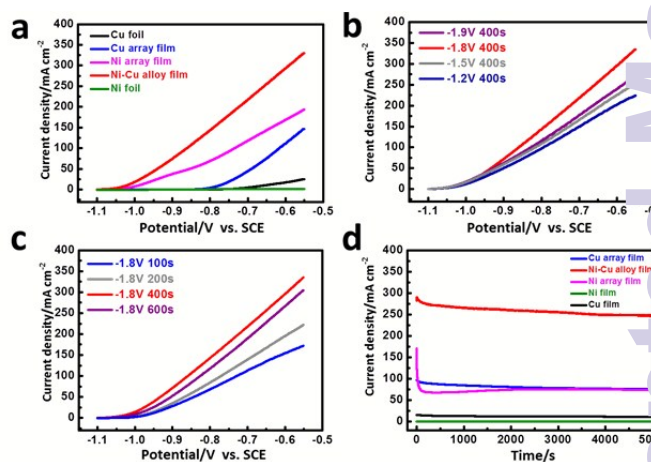


Fig. 4 HzOR performances of the Ni-Cu alloy films in the aqueous electrolyte containing 0.1 mol L⁻¹ N₂H₄·H₂O and 3.0 mol L⁻¹ NaOH: a) Polarization curves of the Ni-Cu alloy film, Cu array film, Ni array film, Cu foil and Ni foil; b) Polarization curves of the Ni-Cu alloy films prepared at different electrodeposition potentials for 400 s; c) Polarization curves of the Ni-Cu alloy films prepared at -1.8 V for different electrodeposition times; d) stability curves of the Ni-Cu alloy film, Cu array film, Ni array film, Cu foil and Ni foil.

To reveal the “intrinsic properties” that dominating the excellent electrocatalyst performance of the Ni-Cu alloy film, we studied and discussed the reaction process of HzOR in our system. Electrochemical impedance spectroscopy (EIS) is usually considered as a powerful tool to study the electrode kinetics in catalytic reactions.⁴² The EIS plots of the Ni-Cu alloy film and control samples are shown in Fig. 5a. The presence of these similar semicircles suggested that the HzOR over these electrocatalysts was kinetically controlled, while the varied diameters of these semicircles indicated different charge transfer resistances (*R*_{ct}). By comparison with these control samples, the 3D porous Ni-Cu alloy film possessed the smallest *R*_{ct}, demonstrating its accelerated kinetics for HzOR. As shown in Fig. 5b, all of the Ni-Cu alloy films prepared under different conditions showed small *R*_{ct} values for HzOR, in which

sample prepared at -1.8 V for 400 s displayed the smallest one, consistent with the structural and catalytic properties of these porous films. Considering the distinct difference in R_{ct} and activity between the nanostructured films and planar foils, it was concluded that the 3D porous structure was important for high performance of the Ni-Cu alloy film, which was probably related to enhanced specific surface area, active site accessibility and molecular/ion diffusion in highly porous nanostructures. Generally, the different adhesive property of catalysts would lead to different gas releasing behavior in gas evolution reaction (like HzOR). In adhesion force measurements, the Ni-Cu alloy film, along with Ni array film and Cu array film, showed negligible adhesion response to the produced gas bubbles (below the detection limit, **Fig. 5c**) and underwater “superaerophobic” surface, different from the high adhesion force between the Ni or Cu foil and the gas bubble, suggesting the importance of constructing highly porous surface for alleviating the gas bubble adhesion.⁴³ The gas bubbles generated on the Ni-Cu alloy film left quickly before they grew larger than $20\ \mu\text{m}$ in diameter (**Fig. 5d** and **Movie S1**). Compared with these on the planar counterparts (**Fig. S5**), the gas bubbles appeared densely and uniformly on the nanostructured surface, suggesting that more active sites were exposed and well distributed. Thus constructing a highly porous nanostructure with a “superaerophobic” surface was crucial to promote the gas evolution behavior in HzOR, and thereby might circumvent the negative effects caused by the bubble adhesion in DHFCs. In addition, $R_{ct(\text{Ni array})}$ was larger than $R_{ct(\text{Cu array})}$, but the HzOR activity of Ni array film was more effective compared to that of Cu array film owing to the intrinsic activity of Ni. It should be pointed out that though the R_{ct} values of the Ni-Cu alloy and Cu array films were similar, the HzOR performance of the binary alloy film was superior to the Cu array and even Ni array films (**Fig. 4a**), suggesting the importance of the binary component.^{34, 35}

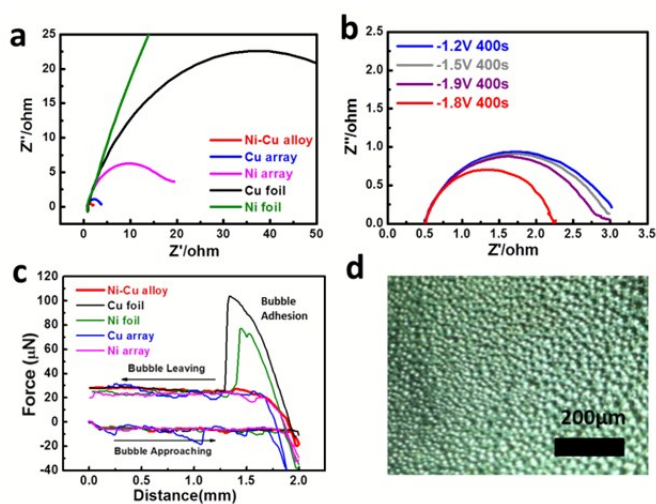


Fig. 5a) Nyquist plots of the Ni-Cu alloy film, Cu array film, Ni array film, Cu foil and Ni foil; **b)** Nyquist plots of the Ni-Cu alloy films prepared at different electrodeposition potentials for 400 s; **c)** Adhesive force measurements of the gas bubbles on

planar and nanostructured films; **d)** the digital image showing the bubble generation behavior on the Ni-Cu alloy film.

Conclusions

The 3D porous Ni-Cu alloy film was successfully fabricated on Cu foil substrate through one-step electrodeposition process. The characterization results confirmed that the Ni-Cu film had a $\text{Ni}_{0.43}\text{Cu}_{0.57}$ alloy component and porous flower-like array structure. The electrodeposition potential and time were tuned according to the structure and property of Cu-Ni alloy films. The resulting Ni-Cu alloy film was used as anode in hydrazine oxidation reaction under moderate conditions (room temperature and dilute hydrazine), and showed an impressive catalytic performance in alkaline media with a high current density of $300\ \text{mA cm}^{-2}$ and retention rate of 80% after 5000 s, which was better than most of the reported Ni-based electrocatalysts. The excellent catalytic property was considered to be related to the Ni-Cu binary component porous structure and “superaerophobic” surface of the Ni-Cu alloy film. The study revealed the 3D porous Ni-Cu alloy film was one kind of promising anode catalysts for DHFCs.

Acknowledgements

This work was financially supported by the National Natural Science Foundation of China (NSFC), Changjiang Scholars and Innovative Research Team in University (IRT1205), the Fundamental Research Funds for the Central Universities (YS1406).

References

1. A. Serov and C. Kwak, *Applied Catalysis B: Environmental*, 2010, **98**, 1-9.
2. R. Jasinski, *ELECTROCHEMICAL TECHNOLOGY*, 1965, **3**, 129-8.
3. S. Karp and L. Meites, *Journal of the American Chemical Society*, 1962, **84**, 906-912.
4. G. E. Evans and K. V. Kordesch, *Science*, 1967, **158**, 1148-1152.
5. K. Tamura and T. Kahara, *Journal of The Electrochemical Society*, 1976, **123**, 776-780.
6. H.-J. Qiu, H.-T. Xu, L. Liu and Y. Wang, *Nanoscale*, 2015, **7**, 386-400.
7. Y. Ding, Y. Wang, L. Zhang, H. Zhang, C. M. Li and Y. Li, *Nanoscale*, 2011, **3**, 1149-1157.
8. F. Jia, J. Zhao and X. Yu, *Journal of Power Sources*, 2011, **222**, 135-139.
9. A. K. Das, R. K. Layek, N. H. Kim, D. Jung and J. H. Lee, *Nanoscale*, 2014, **6**, 10657-10665.
10. G. Wang, A. Gu, W. Wang, Y. Wei, J. Wu, G. Wang, Y. Zhang and B. Fang, *Electrochemistry Communication*, 2009, **11**, 631-634.
11. Z. Wu, Y. Wu, T. Pei, H. Wang and B. Geng, *Nanoscale*, 2014, **6**, 2738-2745.
12. C.-C. Yang, A. S. Kumar, M.-C. Kuo, S.-H. Chien and J. J. Wu, *Zen, Analytica chimica acta*, 2005, **554**, 66-73.

13. Z. Lu, X. Wu, M. Jiang, J. Wang, J. Liu, X. Lei and X. Sun, *Science China Materials*, 2014, **57**, 59-69.
14. E. Granot, B. Filanovsky, I. Presman, I. Kuras and F. Patolsky, *Journal of Power Sources*, 2012, **204**, 116-121.
15. H. Gao, Y. Wang, F. Xiao, C. B. Ching and H. Duan, *The Journal of Physical Chemistry C*, 2012, **116**, 7719-7725.
16. Z. Lu, M. Sun, T. Xu, Y. Li, W. Xu, Z. Chang, Y. Ding, X. Sun and L. Jiang, *Advanced Materials*, 2015, **27**, 2361-2366.
17. P. Argyropoulos, K. Scott and W. Taama, *Electrochim. Acta*, 1999, **44**, 3575-3584.
18. K. Scott, P. Argyropoulos, P. Yiannopoulos and W. Taama, *Journal of Applied Electrochemistry*, 2001, **31**, 823-832.
19. D. Kong, H. Wang, Z. Lu and Y. Cui, *Journal of the American Chemical Society*, 2014, **136**, 4897-4900.
20. M. S. Faber, M. A. Lukowski, Q. Ding, N. S. Kaiser and S. Jin, *The Journal of Physical Chemistry C*, 2014, **118**, 21347-21356.
21. N. V. Rees and R. G. Compton, *Energy & Environmental Science*, 2011, **4**, 1255-1260.
22. U. Martinez, K. Asazawa, B. Halevi, A. Falase, B. Kiefer, A. Serov, M. Padilla, T. Olson, A. Datye and H. Tanaka, *Physical Chemistry Chemical Physics*, 2012, **14**, 5512-5517.
23. T. Sakamoto, D. Matsumura, K. Asazawa, U. Martinez, A. Serov, K. Artyushkova, P. Atanassov, K. Tamura, Y. Nishihata and H. Tanaka, *Electrochimica Acta*, 2015, **163**, 116-122.
24. R. Silva and T. Asefa, *Advanced Materials*, 2012, **24**, 1878-1883.
25. S.-i. Yamazaki, T. Ioroi, K. Tanimoto, K. Yasuda, K. Asazawa, S. Yamaguchi and H. Tanaka, *Journal of Power Sources*, 2012, **204**, 79-84.
26. L. Q. Ye, Z. P. Li, H. Y. Qin, J. K. Zhu and B. H. Liu, *Journal of Power Sources*, 2011, **196**, 956-961.
27. S. J. Lao, H. Y. Qin, L. Q. Ye, B. H. Liu and Z. P. Li, *Journal of Power Sources*, 2010, **195**, 4135-4138.
28. W. X. Yin, Z. P. Li, J. K. Zhu and H. Y. Qin, *Journal of Power Sources*, 2008, **182**, 520-523.
29. J. Li, W. Tang, J. Huang, J. Jin and J. Ma, *Catalysis Science & Technology*, 2013, **3**, 3155-3162.
30. T. Sakamoto, K. Asazawa, U. Martinez, B. Halevi, T. Suzuki, S. Arai, D. Matsumura, Y. Nishihata, P. Atanassov and H. Tanaka, *Journal of Power Sources*, 2013, **234**, 252-259.
31. T.-Y. Jeon, M. Watanabe and K. Miyatake, *ACS applied materials & interfaces*, 2014, **6**, 18445-18449.
32. J. Li, W. Tang, H. Yang, Z. Dong, J. Huang, S. Li, J. Wang, J. Jin and J. Ma, *RSC Advances*, 2014, **4**, 1988-1995.
33. H. Yang, X. Zhong, Z. Dong, J. Wang, J. Jin and J. Ma, *RSC Advances*, 2012, **2**, 5038-5040.
34. T. Sakamoto, K. Asazawa, J. Sanabria-Chinchilla, U. Martinez, B. Halevi, P. Atanassov, P. Strasser and H. Tanaka, *Journal of Power Sources*, 2014, **247**, 605-611.
35. H. Wang, Y. Ma, R. Wang, J. Key, V. Linkov and S. Ji, *Chemical Communications*, 2015, **51**, 3570-3573.
36. K. Kim and N. Winograd, *Surface Science*, 1974, **43**, 625-643.
37. K. Kishi and T. Fujita, *Surface Science*, 1990, **227**, 107-113.
38. N. McIntyre and M. Cook, *Analytical Chemistry*, 1975, **47**, 2208-2213.
39. L. Martin, H. Martinez, D. Poinot, B. Pecquenard and F. d. r. Le Cras, *The Journal of Physical Chemistry C*, 2013, **117**, 4421-4430.
40. V. X. Hien, J.-L. You, K.-M. Jo, S.-Y. Kim, J.-H. Lee, J.-J. Kim and Y.-W. Heo, *Sensors and Actuators B: Chemical*, 2014, **202**, 330-338.
41. R. S. Gonçalves, D. S. Azambuja and A. M. S. Lucho, *Corrosion science*, 2002, **44**, 467-479.
42. D. Merki, H. Vrubel, L. Rovelli, S. Fierro and X. Hu, *Chemical Science*, 2012, **3**, 2515-2525.
43. Z. Lu, W. Zhu, X. Yu, H. Zhang, Y. Li, X. Sun, X. Wang, F. Wang, J. Wang and J. Luo, *Advanced Materials*, 2014, **26**, 2683-2687.